Chapter 3

Multiwavelets and Balancing

When a multiresolution analysis is generated using multiple scaling functions and wavelet functions, it gives rise to the notion of *multiwavelets* . A multiwavelet with r scaling functions and r wavelet functions is said to have multiplicity 'r '. When $r = 1$, one scaling function and one wavelet function, the multiwavelet system reduces to the scalar wavelet system discussed in Chapter 2. In the following exposition we consider multiwavelets with $r = 2$.

The perfect reconstruction multiwavelet filter bank employs 2×2 matrix filters that provide extra degrees of freedom in the design. So unlike scalar wavelets, multiwavelets can be designed to possess the orthogonality and symmetry properties simultaneously. This is a desirable feature for many signal processing applications, including image compression.

As dicussed in Chapter 2, we implement the 2-D wavelet transform as two separable 1-D transforms. The 2×2 matrix filters in our multiwavelet filter bank require vector inputs (discussed in Section 3.1.1). Thus, a 1-D input signal must be transformed into two 1-D signals. This transformation is called pre-processing. For some multiwavelets, the pre-processing must be accompanied by an appropriate pre-filtering operation that depends on the spectral characteristics of the multiwavelet filters [25]. However, some multiwavelets obviate the pre-filtering (and the pre-processing) operation due to certain desirable properties

of their basis functions; these multiwavelets are called *balanced multiwavelets* [10].

In this chapter, the basic multiwavelet theory is presented and then extended to balanced multiwavelets. Finally, the 2-D multiwavelet transform is described for images.

3.1 Multiwavelet Theory

Multiwavelet bases of multiplicity 2 provide a multiresolution analysis $\{V_n\}_{n\in\mathcal{Z}}$ of L^2 using the multiscaling function $\bar{\Phi}(t) = [\phi_0(t), \phi_1(t)]^\top$ and multiwavelet function $\bar{\Psi}(t) = [\psi_0(t), \psi_1(t)]^\top$. The j^{th} scaling space is given by

$$V_j = \underset{k \in \mathcal{Z}}{Span} \{\phi_0(2^j t - k), \phi_1(2^j t - k)\} \tag{3.1}$$

and the j^{th} wavelet space is given by

$$W_j = \underset{k \in \mathcal{Z}}{Span} \{\psi_0(2^j t - k), \psi_1(2^j t - k)\} \tag{3.2}$$

where $V_j \perp W_j$. For the case where $r = 2$, the multiscaling function satisfies the following 2-scale equation

$$\bar{\Phi}(t) = \sqrt{2} \sum_{k=0}^{l-1} H[k] \bar{\Phi}(2t - k) \tag{3.3}$$

where the matrix filter $H[k]$ has l 2×2 matrix coefficients; the k_{th} matrix coefficient is given by

$$H[k] = \begin{bmatrix} h_0(2k) & h_0(2k+1) \\ h_1(2k) & h_1(2k+1) \end{bmatrix} \tag{3.4}$$

such that $\sum_k h_0(k)^2 = 1$ and $\sum_k h_1(k)^2 = 1$. The corresponding multiwavelet function satisfies the following equation

$$\bar{\Psi}(t) = \sqrt{2} \sum_{k=0}^{l-1} G[k] \bar{\Phi}(2t - k) \tag{3.5}$$

where the matrix filter $G[k]$ has l 2×2 matrix coefficients; the k_{th} matrix coefficient is given by

$$G[k] = \begin{bmatrix} g_0(2k) & g_0(2k+1) \\ g_1(2k) & g_1(2k+1) \end{bmatrix} \tag{3.6}$$

such that $\sum_k g_0(k)^2 = 1$ and $\sum_k g_1(k)^2 = 1$.

For the balanced multiwavelets (to be discussed in the following sections), h_0 and h_1 are lowpass FIR filters while, g_0 and g_1 are bandpass or highpass FIR filters.

The perfect reconstruction multiwavelet filter bank is shown in Figure 3.1. If coefficients $\bar{s}_0$

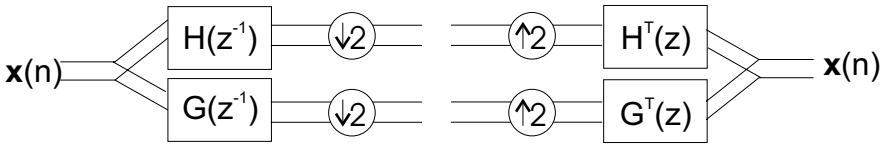

Figure 3.1: The perfect reconstruction multiwavelet filter bank (a) analysis section, (b) synthesis section.

(at scale zero) are input to the analysis section of the filter bank, one iteration computes the coarse vector coefficients $\bar{s}_{-1}$ and the detail vector coefficients $\bar{d}_{-1}$ at scale 2^{-1} as shown in equations (3.7) and (3.8), respectively. This decomposition corresponds to the discrete multiwavelet transform (similar to the DWT in equation (2.10)).

$$\bar{s}_{-1}[n] = \sum_k H[k-2n]\bar{s}_0[k], \tag{3.7}$$

$$\bar{d}_{-1}[n] = \sum_k G[k-2n]\bar{s}_0[k]. \tag{3.8}$$

The corresponding synthesis equation reconstructs $\bar{s}_0$ from $\bar{s}_{-1}$ and $\bar{d}_{-1}$ using equation (3.9). This corresponds to the inverse discrete multiwavelet transform and is equivalent to the IDWT in equation (2.9).

$$\bar{s}_0[n] = \sum_k H^\top[n-2k]\bar{s}_{-1}[k] + \sum_k G^\top[n-2k]\bar{d}_{-1}[k]. \tag{3.9}$$

3.1.1 Pre-processing the Input

The lowpass filter H and highpass filter G in the multiwavelet filter bank are 2×2 matrices. Thus, they need to be convolved with two rows of data. (In fact, in equation (3.7), the

input to the filter bank, $\bar{s}_0$ is a vector). However, for 1-D signals, we have only one row of data; so we have to pre-process the 1-D signal to obtain two rows of data. We note that, the pre-processing should not destroy orthogonality and/or symmetry of the bases. One solution to this problem is simply to repeat the input [10, 24]. But this solution is equivalent to oversampling and results in an expansive technique that is not suitable for compression. Besides, it increases the computational complexity of the transform. Another approach is to split the input into two polyphase components, thereby maintaining critical sampling [10]. This approach is used in this thesis for image compression and is discussed further in Section 3.1.3.

Similar to a scalar filter bank, the lowpass branches in a multiwavelet filter bank should *preserve* some polynomial inputs while the highpass branches should completely *annihilate* them. The annihilation property of the multiwavelet filter bank depends on its approximation order; the approximation order is 'K' if all its wavelets have K vanishing moments.

$$\int t^{\mathsf{m}} \Psi_{\mathsf{i}}(t) \mathrm{d}t = 0, i = 0, 1, \quad 0 \leq m \leq K - 1 \tag{3.10}$$

In order for the preservation property to hold, the polynomial inputs should be eigensignals of the lowpass branch. The band-Toeplitz matrix for the lowpass branch of the multiwavelet filter bank is given by equation (3.11).

$$L = \begin{bmatrix} H[0] & H[1] & H[2] & H[3] & \cdots & H[l] & & & \\ & & H[0] & H[1] & H[2] & H[3] & \cdots & H[l] & \\ & & & & H[0] & H[1] & H[2] & H[3] & \cdots & H[l] \end{bmatrix} \tag{3.11}$$

where, $H[0], H[1], H[2], H[3], \cdots, H[l]$ are the matrix coefficients of the matrix lowpass filter H [11].

If the zero-order polynomial $x = [\cdots, 1, 1, 1, 1 \cdots]$ is preserved by the lowpass branch, x is an eigensignal of the lowpass branch — see equation (3.12). Such a multiwavelet is said to be *balanced* to order 1 [10].

$$L[\cdots, 1, 1, 1, 1 \cdots]^\top = [\cdots, 1, 1, 1, 1 \cdots]^\top. \tag{3.12}$$

When the multiwavelet filter bank possesses the preservation/annihilation property for higher order input polynomials, it is said to have a higher balancing order.

Not all multiwavelets are balanced. We refer to such multiwavelets as *unbalanced multiwavelets*. For the GHM (Geronmo-Hardin-Massopust) multiwavelet, when the polyphase components of a dc signal are fed to the lowpass branch, it fails to preserve it [7]. The result shown in Figure 3.2(a) indicates that the zero-order polynomial is not its eigensignal. Equation 3.13 shows that $x = [..., 1, \sqrt{2}, 1, \sqrt{2}...]$ is an eigensignal of the lowpass branch and is preserved by it (Figure 3.2(b)). Thus, the GHM multiwavelet is unbalanced. The lack of balancing in its filter bank is compensated for by pre-filtering the dc input and converting it into the eigensignal of the lowpass branch of the filter bank; this pre-processing is not desirable due to the increased computational complexity. Similarly, for other unbalanced multiwavelets like Chui-Lian, there are suitable pre-filtering techniques [5, 24].

$$L[\cdots, 1, \sqrt{2}, 1, \sqrt{2} \cdots]^\top = [\cdots, 1, \sqrt{2}, 1, \sqrt{2} \cdots]^\top. \tag{3.13}$$

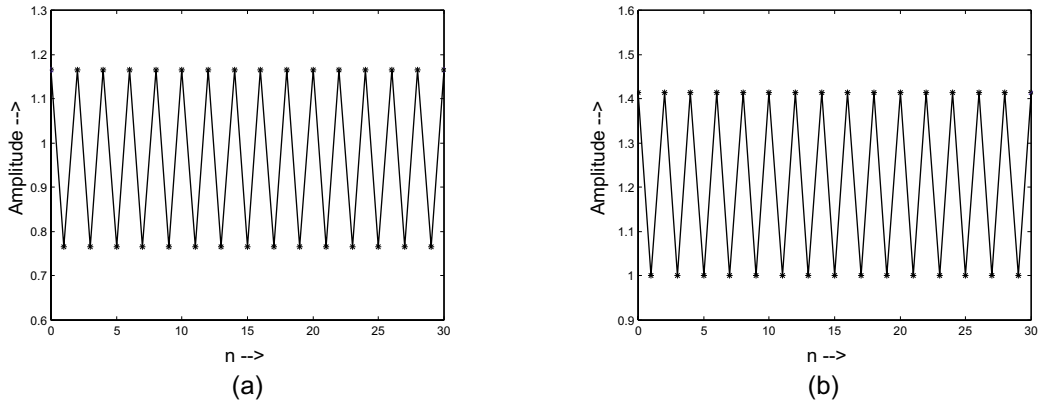

Figure 3.2: Decomposition using GHM multiwavelet (a) lowpass branch output for dc input ($x = [1, 1, 1, \cdots]$), (b) lowpass branch output for the eigensignal input ($x = [\cdots 1, \sqrt{2}, 1, \sqrt{2} \cdots]$).

3.1.2 Balanced Multiwavelets

In general, for multiwavelets, the preservation property does not automatically follow from the vanishing moments property. But, for the balanced multiwavelet filter banks, both the preservation and annihilation properties hold. The balanced multiwavelets do not require a pre-processing stage (other than polyphase vectorization[1]) for the input. If the lowpass/highpass branches of the filter bank preserve/annihilate polynomials of order less than p where $p \leq K$, then the balancing order for the multiwavelet is p. A balancing order of p implies at least p vanishing moments; it also implies that $(0^{\text{th}}, 1^{\text{st}}, 2^{\text{nd}}\cdot, \cdot, \cdot(p-1)^{\text{th}})$ order polynomials are eigensignals of the lowpass branch band-Toeplitz matrix.

Figure 3.3 shows the lowpass and highpass branch outputs of a multiwavelet filter bank balanced to order 2 for zero-order (dc), first order (ramp) and second order (quadratic) inputs. It is seen that the zero and first order monomials are preserved at the lowpass output while they are annihilated by the highpass branch. We note that, the drop-off in the output signal end-points in Figures 3.3 (b), (d) and (f) is due to the abrupt cut-off at the input signal end-point. Figures 3.3 (e), (f) show that the second order monomial is not preserved/annihilated by the filter bank.

[1] It will be seen in section 3.1.3 that an alternate representation of the multiwavelet filter bank eliminates the polyphase vectorization stage also.

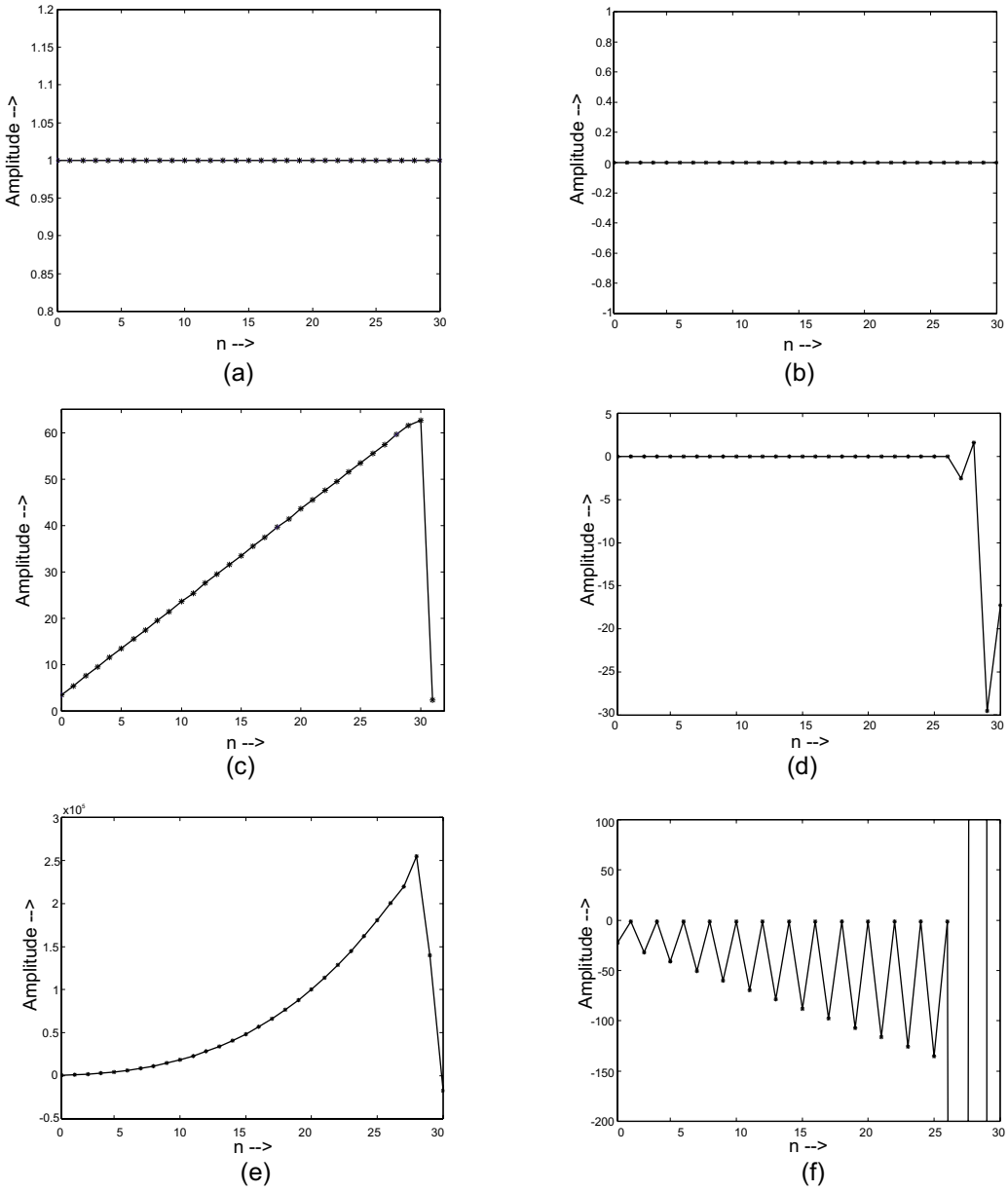

Figure 3.3: Decomposition using a 2^{nd} order balanced multiwavelet (a) lowpass branch output for dc input ($x = [1, 1, 1, \cdots]$), (b) highpass branch output for the dc input, (c) lowpass branch output for a ramp input ($x = [1, 2, 3, \cdots]$), (d) highpass branch output for the ramp input, (e) lowpass branch output for quadratic input ($x = [1^2, 2^2, 3^2, \cdots]$), (f) highpass branch output for the quadratic input.

3.1.3 The Time-varying Multiwavelet Filter Bank

Polyphase vectorization of the input reduces the matrix filter bank into a simple multichannel filter bank [10, 27]. Equations (3.14) and (3.15) give the filters for the multichannel filter bank. Here, $H_0(z)$ and $H_1(z)$ are the $\mathcal{Z}$-transforms of the two lowpass branch filters h_0 and h_1 in equation (3.4). They replace the lowpass matrix filter $H(z)$ in the matrix filter bank of Figure 3.1. Similarly, $G_0(z)$ and $G_1(z)$ are the $\mathcal{Z}$-transforms of the two highpass branch filters g_0 and g_1 in equation (3.6). They replace the highpass matrix filter $G(z)$ in the matrix filter bank.

$$\begin{bmatrix} H_0(z) \\ H_1(z) \end{bmatrix} = H(z^2) \begin{bmatrix} 1 \\ z^{-1} \end{bmatrix}, \tag{3.14}$$

$$\begin{bmatrix} G_0(z) \\ G_1(z) \end{bmatrix} = G(z^2) \begin{bmatrix} 1 \\ z^{-1} \end{bmatrix}. \tag{3.15}$$

Thus the 2×2 matrix filters H and G in the multiwavelet filter bank of Figure 3.1 are rearranged to form a 4-channel filter bank with simple filters in Figure 3.4. This arrangement requires simple 1-D inputs. Thus it eliminates the need for vectorization of the input. As will be seen in the following section, if the branch filters have similar spectral characteristics (true for balanced multiwavelets), the downsampler outputs are interleaved before the further decomposition.

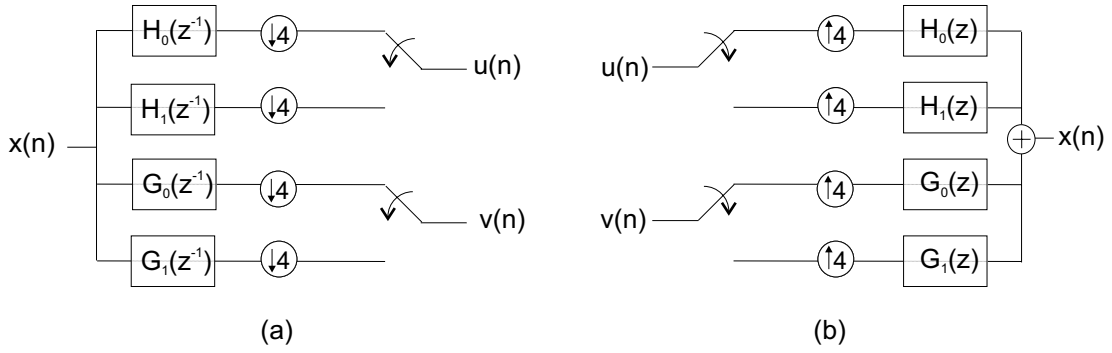

Figure 3.4: The time-varying multiwavelet filter bank (a) analysis section, (b) synthesis section.

This interleaving operation (if applicable) makes this multichannel multiwavelet filterbank different from the 4-channel scalar filter bank. In each branch in the multiwavelet filter bank, the downsampler outputs contribute to alternate samples in the interleaved signal. The time-shift of the downsampler outputs determines which filter's output samples will precede the other in the interleaved signal; even and odd time-shifted outputs from the downsampler give different signals after interleaving. Thus, interleaving accounts for the time-variance of the system.

The multichannel multiwavelet filter bank representation is convenient because it allows us to analyze the multiwavelet implementation (as will be seen in Chapter 4) along the same lines as the multichannel scalar wavelet filter bank [23] which is well understood.

In the case of unbalanced multiwavelets, the outputs of the time-varying filter bank are not interleaved prior to further signal processing due to widely different spectral characteristics of its branch filters. The spectral characteristics of balanced and unbalanced multiwavelets are explored further in Chapter 4.

3.2 The 2-D Multiwavelet Decomposition

The separable 2-D multiwavelet transform is performed as a 1-D row transform followed by a 1-D column transform. Figure 3.5 shows the multiwavelet filter bank for a single-level 2-D decomposition for $r = 2$. The sixteen subbands generated after the row and column transformations are indicated in the figure. Prior to encoding with *SPIHT*, the subbands are arranged as shown in Figure 3.6 [25]. (The subbands are denoted by $X_{\mathrm{i}}Y_{\mathrm{j}}$ where, $X, Y = L, H$; L and H correspond to lowpass and highpass outputs, respectively; the subscripts $i, j = 0, 1$ correspond to the filters in branch X or Y). This kind of subband structure destroys the parent-child dependency that the *SPIHT* quantizer exploits. In the following subsections, a procedure which restores the spatial dependencies is explained.

For unbalanced multiwavelets, a one-level decomposition shows that a large amount of simi-

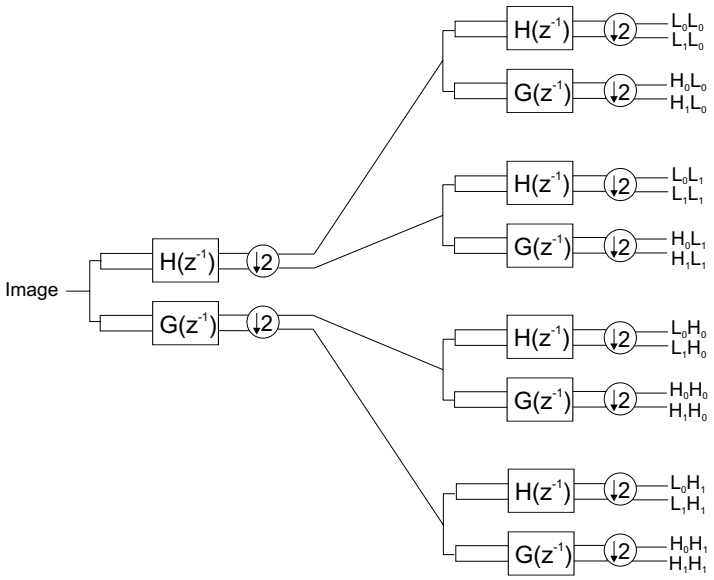

Figure 3.5: The 2-D multiwavelet filter bank.

larity exists in the 2×2 blocks that comprise the $L_{\mathrm{i}}H_{\mathrm{j}}$, $L_{\mathrm{i}}H_{\mathrm{j}}$ and $H_{\mathrm{i}}H_{\mathrm{j}}$ subbands. To restore the spatial dependencies, we interleave the high frequency subbands $X_{\mathrm{i}}Y_{\mathrm{j}}$ ($X_{\mathrm{i}}Y_{\mathrm{j}} \neq L_{\mathrm{i}}L_{\mathrm{j}}$) into a single block XY. Thus, blocks *LH, HL* and *HH* are generated. This interleaving procedure is called *shuffling* [14]. Figure 3.7 shows how the $X_{\mathrm{i}}Y_{\mathrm{j}}$ subbands are shuffled into the block XY. The coefficients 1-4 map to a 2×2 set of adjacent coefficients in the shuffled block, as do coefficients 5-8. Thus, shuffling restores the dispersed children into 2×2 blocks.

For the unbalanced multiwavelets, the $L_{\mathrm{i}}L_{\mathrm{j}}$ subbands have dissimilar spectral characteristics.

L_0L_0	L_1L_0	L_0H_0	L_1H_0
L_0L_1	L_1L_1	L_0H_1	L_1H_1
H_0L_0	H_1L_0	H_0H_0	H_1H_0
H_0L_1	H_0L_0	H_0H_1	H_1H_1

Figure 3.6: Single-level multiwavelet decomposition showing 16 subbands.

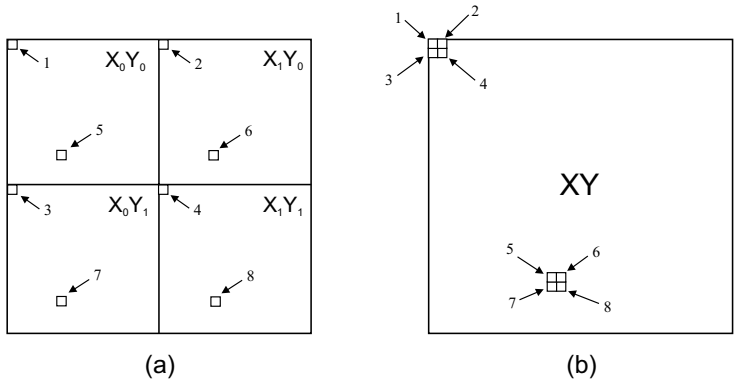

Figure 3.7: Subband structure (a) before shuffling, (b) after shuffling.

So they are not shuffled.

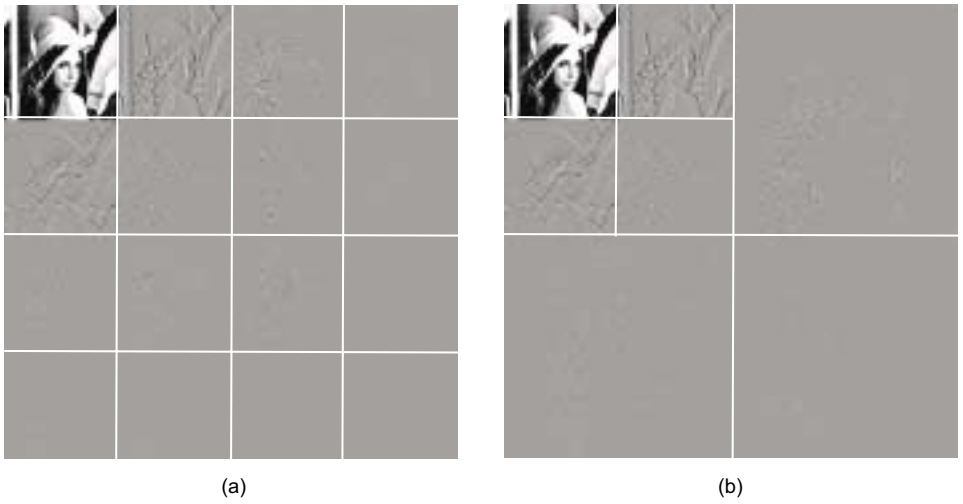

Figure 3.8: Single-level unbalanced multiwavelet decomposition (a) before shuffling, (b) after shuffling.

Figure 3.8 shows an example of a one-level unbalanced multiwavelet decomposition before and after shuffling. We note that the subband structure of the shuffled decomposition is equivalent to a two-level scalar wavelet decomposition. Amongst the $L_{\mathrm{i}}L_{\mathrm{j}}$ subbands, only the L_0L_0 subband is an approximation of the original image; so, we iteratively decompose L_0L_0 to form the scale-space pyramid. In terms of the subband structure, three levels of

decomposition using an unbalanced multiwavelet, with shuffling is roughly equivalent to a 5-level scalar wavelet decomposition [14].

An important difference to note between unbalanced and balanced multiwavelets is that, for balanced multiwavelets, in addition to the other subbands, the $L_{\mathrm{i}}L_{\mathrm{j}}$ subbands also have similar spectral characteristics [11]. Therefore, we shuffle all of the subbands $X_{\mathrm{i}}Y_{\mathrm{j}}$ $(X, Y = L, H$ and $i, j = 0, 1)$ in Figure 3.6 into a single block, XY. Thus, the shuffled one-level *balanced* multiwavelet decomposition consists only of four subbands *LL, HL, LH* and *HH*; this is similar to the one-level scalar wavelet deomposition of Figure 2.4. The equivalent time-varying balanced multiwavelet filter bank is shown for a single-level, 2-D transform in Figure 3.9.

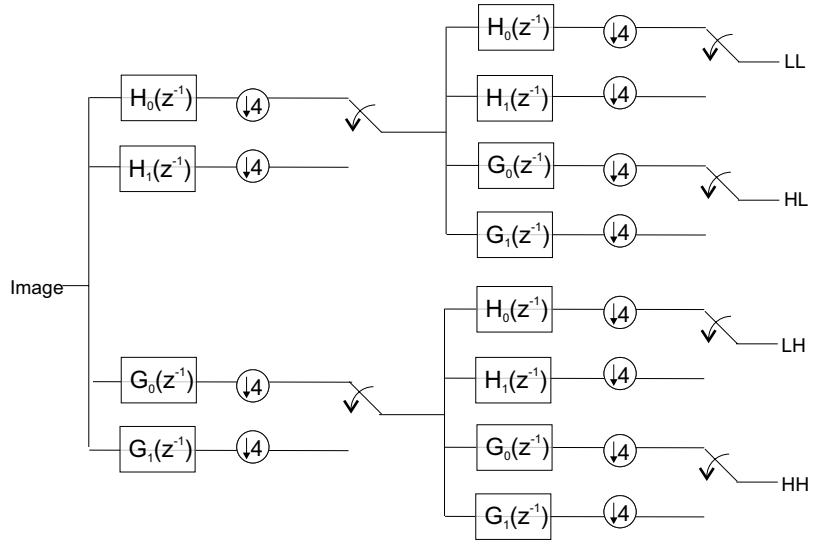

Figure 3.9: The 2-D balanced multiwavelet filter bank.

Figure 3.10 shows the image *Lena* before and after shuffling is applied to a one-level balanced multiwavelet decomposition. The shuffled one-level balanced multiwavelet decomposition has the same subband structure as Figure 2.4. We iterate on the shuffled LL block to form the subband pyramid and then quantize the coefficients with *SPIHT*.

Figure 3.10: Single-level balanced multiwavelet decomposition (a) before shuffling, (b) after shuffling.